Experimental Minimum-Error Quantum-State Discrimination in High Dimensions

M. A. Solís-Prosser,[1,2,*] M. F. Fernandes,[3] O. Jiménez,[4] A. Delgado,[1,2] and L. Neves[3,†]
[1]*Center for Optics and Photonics and MSI-Nucleus on Advanced Optics, Universidad de Concepción, Casilla 4016, Concepción, Chile*
[2]*Departamento de Física, Universidad de Concepción, Casilla 160-C, Concepción, Chile*
[3]*Departamento de Física, Universidade Federal de Minas Gerais, Belo Horizonte, MG 31270-901, Brazil*
[4]*Departamento de Física, Facultad de Ciencias Básicas, Universidad de Antofagasta, Casilla 170, Antofagasta, Chile*

(Received 19 April 2016; published 6 March 2017)

Quantum mechanics forbids perfect discrimination among nonorthogonal states through a single shot measurement. To optimize this task, many strategies were devised that later became fundamental tools for quantum information processing. Here, we address the pioneering minimum-error (ME) measurement and give the first experimental demonstration of its application for discriminating nonorthogonal states in high dimensions. Our scheme is designed to distinguish symmetric pure states encoded in the transverse spatial modes of an optical field; the optimal measurement is performed by a projection onto the Fourier transform basis of these modes. For dimensions ranging from $D = 2$ to $D = 21$ and nearly 14 000 states tested, the deviations of the experimental results from the theoretical values range from 0.3% to 3.6% (getting below 2% for the vast majority), thus showing the excellent performance of our scheme. This ME measurement is a building block for high-dimensional implementations of many quantum communication protocols, including probabilistic state discrimination, dense coding with nonmaximal entanglement, and cryptographic schemes.

DOI: 10.1103/PhysRevLett.118.100501

Quantum mechanics establishes fundamental bounds to our capability of distinguishing among states with nonvanishing overlap: if one is given at random one of two or more nonorthogonal states and asked to identify it from a single shot measurement, it will be impossible to accomplish the task deterministically and with full confidence. This constraint has deep implications both foundational, underlying the debate about the epistemic and ontic nature of quantum states [1–4], and practical, warranting secrecy in quantum key distribution [5,6]. Beyond that, the problem of discriminating nonorthogonal quantum states plays an important role in quantum information and quantum communications [7].

A wide variety of measurement strategies have been devised in order to optimize the state discrimination process according to a predefined figure of merit [7]. The pioneering one was the minimum-error (ME) measurement [8–10] where each outcome identifies one of the possible states and the overall error probability is minimized. Other fundamental strategies conceived later [11–17] employ the ME discrimination in the step next to a transformation taking the input states to more distinguishable ones [18], which enables us to identify them with any desired confidence level (within the allowed bounds) and a maximum success probability. Nowadays, the ME measurement is central to a range of applications, including quantum imaging [19], quantum reading [20], image discrimination [21], error correcting codes [22], and quantum repeaters [23], thus stressing its importance.

Closed-form solutions for ME measurements are known only for a few sets of states. One of these is the set of symmetric pure states (defined below) prepared with equal prior probabilities [24]. Discriminating among them with minimum error sets the bounds on the eavesdropping in some quantum cryptographic schemes [25] and is crucial for optimal deterministic and probabilistic realizations of protocols like quantum teleportation [26], entanglement swapping [27], and dense coding [28], when the quantum channels are nonmaximally entangled.

Experimental demonstrations of ME discrimination have been provided in continuous variables for two coherent states [29], and in two-dimensional Hilbert spaces for sets of two [30], three, and four states [31] encoded in the light polarization, and two states encoded in the ^{14}N nuclear spin [32]. It is of key importance to extend this to high-dimensional quantum systems (qudits) due to the many advantages they offer over qubit-based applications. Qudits provide an increase in the channel capacity for quantum communication [33], and a higher error rate tolerance and improved security in quantum key distribution [34–36]. Moreover, they are a necessary resource for fundamental tests of quantum mechanics, like contextuality tests [37], and for lowering the detection efficiencies required for nonlocality tests [38]. Therefore, the ability to perform ME measurements for qudit states will enhance their potential of use in many of these practical applications. It will also be essential for exploring novel protocols of quantum-state discrimination [14–16], bringing positive impacts for quantum communications.

In this Letter, we report the first experimental demonstration of ME discrimination among nonorthogonal states of a single qudit. This is done for equally likely symmetric states in dimensions D ranging from $D = 2$ to $D = 21$. Using states encoded in D transverse spatial modes of an optical field, known as spatial qudits [39], we carried out the experiment for every dimension in that range in a total of 1851 sets of states. Up to small deviations caused by unavoidable experimental imperfections, our scheme is shown to be optimal, achieving the minimum error probability allowed by quantum mechanics.

To outline the problem, consider a set of N quantum states $\{|\psi_j\rangle\}_{j=0}^{N-1}$ spanning a D-dimensional Hilbert space $\mathcal{H}_D$, with $D \leq N$, defined by

$$|\psi_j\rangle = \sum_{n=0}^{D-1} c_n \omega^{jn} |n\rangle, \qquad (1)$$

where $\omega = \exp(2\pi i/N)$, the c_n's are real and nonnegative $(\sum_n c_n^2 = 1)$, and $\{|n\rangle\}_{n=0}^{D-1}$ is an orthonormal basis in $\mathcal{H}_D$. They are symmetric under $\hat{U} = \sum_{l=0}^{D-1} \omega^l |l\rangle\langle l|$ since $|\psi_j\rangle = \hat{U}|\psi_{j-1}\rangle = \hat{U}^j|\psi_0\rangle$ and $|\psi_0\rangle = \hat{U}|\psi_{N-1}\rangle$. If each of these states is prepared with the same *a priori* probability $1/N$, they can be identified with minimum error through the measurement [24]

$$\hat{\Pi}_k^{\mathrm{ME}} = \hat{\mathcal{F}}_N |k\rangle\langle k| \hat{\mathcal{F}}_N^{-1} \equiv |\mu_k\rangle\langle\mu_k|, \qquad (2)$$

where $k = 0, \ldots, N-1$, and $\hat{\mathcal{F}}_N = (1/\sqrt{N}) \sum_{m,n=0}^{N-1} \omega^{mn} |m\rangle\langle n|$ is the discrete Fourier transform acting on an N-dimensional Hilbert space $\mathcal{H}_N$. For $N = D$ (linearly independent states), this is a projective measurement on $\mathcal{H}_D$. For $N > D$ (linearly dependent states), this is a projective measurement on $\mathcal{H}_N$ that realizes the positive operator valued measure (POVM) for ME discrimination on $\mathcal{H}_D$. This procedure is based on Neumark's theorem [10] for implementing POVMs by embedding the system space $\mathcal{H}_D$ into a larger Hilbert space $\mathcal{H}_N$ given by the direct sum $\mathcal{H}_D \oplus \mathcal{H}_{N-D}$, where $\mathcal{H}_{N-D}$ represents the $N - D$ unused extra dimensions of the original system [40]. From Eqs. (1) and (2), the probability of obtaining an outcome δ_k (associated with $\hat{\Pi}_k^{\mathrm{ME}}$) if the prepared state was $|\psi_j\rangle$ is given by $P(\delta_k|\psi_j) = |\langle\mu_k|\psi_j\rangle|^2$. Thus, the maximum overall probability of correctly identifying the state will be

$$P_{\mathrm{corr}} = \frac{1}{N} \sum_{j=0}^{N-1} P(\delta_j|\psi_j) = \frac{1}{N} \left(\sum_{j=0}^{D-1} c_j \right)^2. \qquad (3)$$

Equivalently, $P_{\mathrm{err}} = 1 - P_{\mathrm{corr}}$ will be the ME probability.

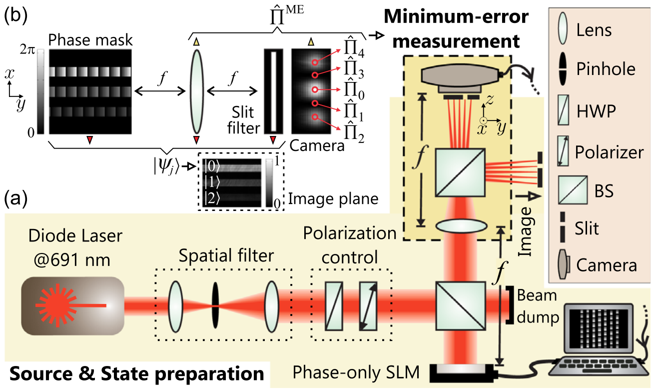

FIG. 1. (a) Experimental setup. Our light source is a single-mode diode laser operating at 691 nm. The beam profile was spatially filtered, expanded, and collimated so that it was approximately a plane wave with constant phase across the screen of the spatial light modulator (SLM). A half-wave plate (HWP) followed by a polarizer provided a clean vertical polarization (the working direction of the SLM) and acted as a variable attenuator to avoid saturation of the detectors. The first 50:50 beam splitter (BS) enabled the normal incidence of the beam onto the reflective phase-only SLM (Holoeye PLUTO). The modulated beam was transmitted through a converging lens ($f = 30$ cm) and split in two arms by the second BS. At each arm a slit diaphragm was placed nearly at the focal plane of the lens in order to select the $+1$ diffraction order where the states were prepared. Note that this BS is not required for the ME measurement; we used it to assist the characterization of the prepared states [41]. In both arms intensity measurements were carried out with CMOS cameras (Thorlabs DCC1545M). The ME measurement was performed in the transmitted arm (dashed box), where the camera was placed at the focal plane of the lens, right behind the slit diaphragm; in the reflected arm, the light distribution was imaged onto the other camera [41]. The SLM and both cameras were connected to a computer that controlled the former and collected and stored data from the latter. (b) Schematic of the state preparation and ME measurement stages (see text for details).

The experimental setup used to optically demonstrate the ME discrimination among symmetric states is shown and described in Fig. 1(a). We use a bright beam from a single-mode laser as our light source, which is usual in most optical implementations of quantum-state discrimination [30,31,48,49]. The transverse spatial profile of this beam is proportional to the transverse probability amplitude of a single-photon multimode field. With the procedure described next, it will mimic the quantum state (1) of a single-photon qudit. The arrangement within the light shaded region enables the preparation of arbitrary pure states of spatial qudits, as recently demonstrated [50]. This is possible by modulating the transverse spatial profile of the incoming field as follows: an array of D rectangular slits with a blazed diffraction grating inside each one is displayed on the screen of the phase-only spatial light modulator. [Figure 1(b) shows a typical phase mask for $D = 3$.] In the back focal plane of a converging lens, the beam portions impinging within the slit zones are diffracted into different orders $(0, \pm 1, \ldots)$; the portions impinging outside the slit zones go to the zeroth diffraction order. If we choose one of the high orders, say $+1$, to prepare the states, the amplitude of their complex coefficients is obtained by controlling the amount of light diffracted by

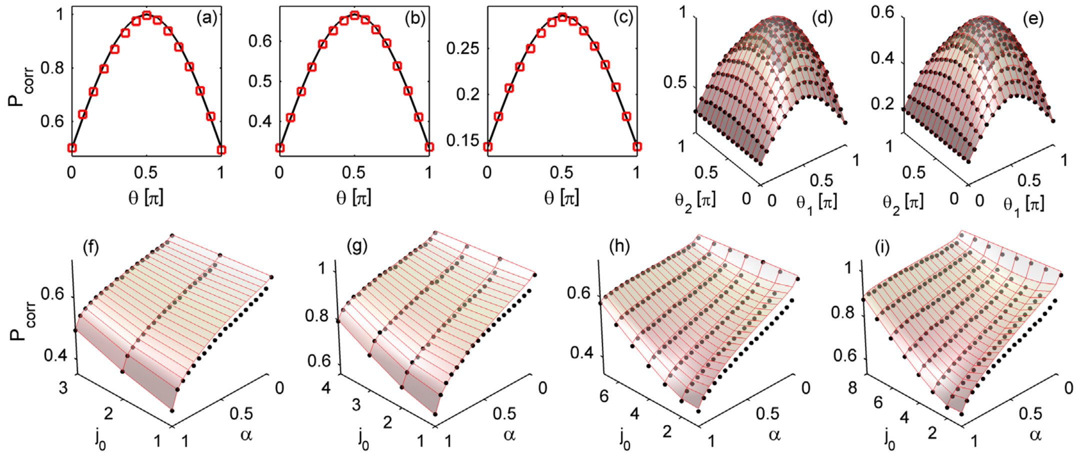

FIG. 2. Optimal probability of correctly identifying the states $P_{\rm corr}$ [Eq. (3)] as a function of their coefficient parameter(s) (see text). Experimental results (squares and points) and theoretical predictions (solid lines and surfaces) of ME discrimination for N states in dimension D ($N \times D$): (a) 2×2, (b) 3×2, (c) 7×2, (d) 3×3, (e) 5×3, (f) 6×4, (g) 5×5, (h) 12×8, (i) 9×9.

each slit to that order, which is a function of the phase modulation depth of the gratings. The relative phases are set either by adding a constant phase value to the gratings [50] or by lateral displacements of them [51] (here we interchanged between these two procedures [41]). Finally, a slit diaphragm filters out the $+1$ diffraction order from the others and the emerging light will be a coherent superposition of the which-slit modes $\{|n\rangle\}_{n=0}^{D-1}$ modulated by proper complex coefficients, thus representing the desired qudit state of Eq. (1). A schematic of the preparation stage is shown in Fig. 1(b). The inset presents an intensity measurement at the image plane for a state $|\psi_j\rangle$ prepared with the phase mask shown there.

The ME measurement is performed through spatial postselection. Let $\hat{\Pi}(x,z) = |\mu(x,z)\rangle\langle\mu(x,z)|$ denote the measurement operator associated with a pointlike detector in the transverse position x and a longitudinal distance $z \in [f, 2f]$ from a converging lens of focal length f. In an N-dimensional space this detector postselects the state $|\mu(x,z)\rangle \propto \sum_{\ell=0}^{N-1} \varphi_\ell(x,z)|\ell\rangle$, where the complex coefficients $\varphi_\ell(x,z)$ are given by the Fresnel diffraction integral of slit ℓ calculated in (x,z) [52]. If the detector is placed at the focal plane of the lens ($z = f$), it will postselect the state $|\mu(x,f)\rangle = (1/\sqrt{N})\sum_{\ell=0}^{N-1} \omega^{xdN\ell/\lambda f}|\ell\rangle$, where d is the slit separation and λ is the light wavelength. Now, consider an array of N detectors at $z = f$ distributed along the transverse positions $x_k = -\lambda f m_k/dN$, where $k = 0, \ldots, N-1$, and $m_k = k$ if $0 \le k \le N/2$ or $m_k = k - N$ if $N/2 < k \le N-1$ [41]. It is easy to see that each detector in this array postselects the state $|\mu(x_k, f)\rangle = \hat{\mathcal{F}}_N|k\rangle$. From Eq. (2), we have

$$\hat{\Pi}(x_k, f) \equiv \hat{\Pi}_k^{\rm ME}, \quad \text{for } x_k = -\lambda f m_k/dN. \tag{4}$$

Therefore, with such a detection scheme we can implement the ME discrimination of symmetric states. From the discussion following Eq. (2), for $N > D$, the D-slit array can be viewed as an array of N slits where D input modes are used to encode the states and the remaining $N - D$ modes are in their respective vacuum states. The propagation through the lens system provides the unitary coupling between these two subspaces and the projective measurement (4) accomplishes the optimal POVM.

In our setup, the ME measurement is shown in the dashed box of Fig. 1(a). Figure 1(b) shows a schematic of this stage with an example of $D = 3$ and $N = 5$. Note that we used the same lens to assist the preparation and measurement stages described above. This was done to simplify the setup, as our main goal was to demonstrate the optimal discrimination process. The same results would be achieved if the detection were performed after letting the spatial qudit state propagate through an arrangement of lenses taking the Fourier transform of the which-slit modes (possibly having to rescale the x_k's).

Our implementation comprised both linearly independent and dependent states in every dimension from $D = 2$ to $D = 21$. Their coefficient amplitudes, $\{c_n\}_{n=0}^{D-1}$ in Eq. (1), were parametrized as follows. For $D = 2$, $c_0 = \cos(\theta/2)$ with $\theta \in [0, \pi]$; for $D = 3$, $c_0 = \sin(\theta_1/2)\cos(\theta_2/2)$ and $c_1 = \sin(\theta_1/2)\sin(\theta_2/2)$ with $\theta_{1(2)} \in [0, \pi]$. These hyperspherical coordinates enabled the experiment to be performed for arbitrary symmetric states in those dimensions. However, for $D \ge 4$, this approach would prevent us to represent the results in a single plot. Thus, for $D = 4$ to 9 we defined $c_n^2 \propto 1 - \sqrt[D]{[(n - j_0 + 1)/(D - j_0)]\alpha}$ if $n \ge j_0$, and $c_n^2 \propto 1$ if $n < j_0$, where $j_0 = 1, \ldots, D-1$ and $\alpha \in [0, 1]$. Using only two parameters (j_0, α) we were able to test a large diversity of sets of symmetric states in those dimensions and, at the same time, to obtain surfaces for the probabilities in Eq. (3) with good contrast [41]. This latter aspect ensured that the tested sets were well distinguishable from one another,

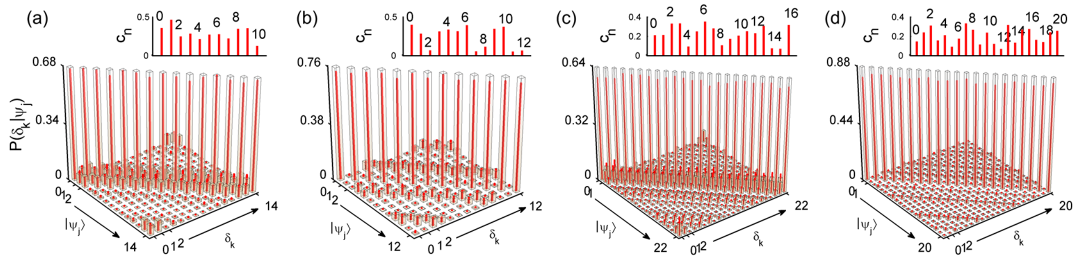

FIG. 3. Probabilities $P(\delta_k|\psi_j)$ in the ME measurement (2) for a set of states defined by the coefficient amplitudes $\{c_n\}_{n=0}^{D-1}$ shown in the inset. Experimental results (red stems) and theoretical predictions (empty bars) for discrimination among N states in dimension D ($N \times D$): (a) 15×11, (b) 13×13, (c) 23×17, (d) 21×21.

since $P_{\rm corr}$ in the ME discrimination is also a measure of distinguishability among sets of states [53]. As D gets larger, to experimentally build up those surfaces became very time consuming. Thus, for $D = 10$ to 21 we found it sufficient to generate a few sets of states (three for each D) to perform the discrimination. In order to avoid any bias in our choice, the coefficients were randomly selected [54].

With the preparation and measurement stages outlined above, the experiment is carried out in the following way: we first define the set of symmetric states by specifying D, N, and the coefficient amplitudes $\{c_n\}_{n=0}^{D-1}$ [Eq. (1)]. Afterwards, we prepare one state of this set and perform the discrimination process on it by measuring, with a CMOS camera, the light intensity at the N transverse positions defined in Eq. (4). This is exemplified in Fig. 1(b). The measured intensities are integrated over y [this direction, also shown in Fig. 1(b), is not relevant for us], the background noise is subtracted, and a small compensation for the detection efficiency due to diffraction is applied [41]. These procedures are repeated for each state in the set. Denoting I_{kj} as the resulting intensity at detector k when the input state is $|\psi_j\rangle$, the probability of identifying it (correctly or incorrectly) is obtained as $[P(\delta_k|\psi_j)]_{\rm expt} = I_{kj}/\sum_{\ell=0}^{N-1} I_{\ell j}$, from which we estimate the overall probability of correct identification, $P_{\rm corr}$, using the expression in the middle of Eq. (3).

In total, the experiment was performed for 1851 sets of symmetric states, comprising nearly 14 000 different states [41]. Figures 2 and 3 show a collection of our results for the values of N and D specified there. In Fig. 2 we plot $P_{\rm corr}$ as a function of the parameter(s) of the state coefficients defined earlier. The experimental results are given by the squares and points while the theoretical predictions—computed from the rightmost side of Eq. (3)—by the solid curves and surfaces. The error bars in these graphs were smaller than the size of the data points. In Fig. 3 we plot $P(\delta_k|\psi_j)$, defined above Eq. (3). Each graph shows these probabilities for a single set of states settled by the coefficient amplitudes shown in the inset. The red stems are the experimental results and the empty bars the expected theoretical values given by $[P(\delta_k|\psi_j)]_{\rm theor} = |\langle\mu_k|\psi_j\rangle|^2$. We observe in both figures the close agreement between theory and experiment.

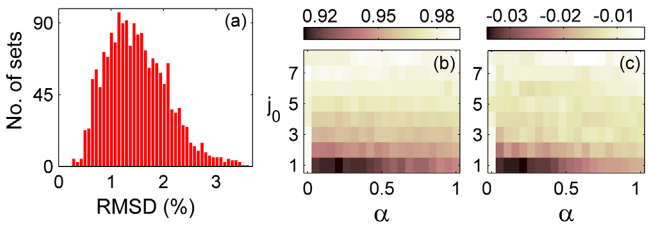

FIG. 4. (a) Histogram with the distribution of the root-mean-square deviations of the experimental results from the theoretical values. (b) Average fidelities of state preparation and (c) RMSD × (−1) for the results shown in Fig. 2(i).

For each of the tested sets we calculated the root-mean-square deviation (RMSD) of the results from the optimal theoretical values. With the residuals defined by $R_{kj} \equiv [P(\delta_k|\psi_j)]_{\rm theor} - [P(\delta_k|\psi_j)]_{\rm expt}$, we have $\text{RMSD} = \sqrt{\sum_{j,k=0}^{N-1} R_{kj}^2/N^2}$. Figure 4(a) shows a histogram of the obtained deviations, which ranged from 0.3% to 3.6%. For 80% of the sets the RMSDs were below 2%. The errors in our experiment are caused mainly by aberrations of the optical elements and the imperfect preparation of the input states, which is, possibly, responsible for the largest deviations. For instance, examining the results of Fig. 2(i), it can be seen that the worse ones occurred for $j_0 = 1$, 2 and some values of $\alpha \neq 0$. For this particular realization, we plot in Figs. 4(b) and 4(c) the average fidelities of preparation for the states in each set and the RMSD×(-1), respectively. It is clearly observed that the largest deviations from the theoretical predictions correspond to the sets of states with lower fidelities. Despite all this, the deviations in our experiment, as shown in Fig. 4(a), were considerably small taking into account that experimental implementations are always subjected to errors, the wide variety of states tested, and the high dimensions we have explored. Therefore, it is safe to say that our scheme is indeed optimal.

In conclusion, we have presented the first experimental demonstration of minimum-error discrimination among nonorthogonal states of a D-dimensional qudit. Our measurement scheme was designed to distinguish symmetric pure states, an important resource in quantum information [12–16,18,24–28]. Envisaging its application to quantum protocols, a single photon implementation of this experiment would require a source with a sufficiently large transverse spatial coherence, in order to prepare high-quality states. The preparation and measurement stages would be exactly the same described earlier. The detector array, however, will be required to have single-photon counting capability. Some candidates for this include charged-coupled device cameras (CCDs), either an intensified CCD [55] or an electron multiplying CCD [56], and also single-photon avalanche diode arrays based on CMOS technology [57,58].

The ME measurement is central not only to many applications in quantum information, but also to put forward the implementation of "complete" probabilistic discrimination protocols in high dimensions: by iterating the discrimination process in case of failed attempts [26], one can significantly increase the information gain about the input states. Our demonstration constitutes a building block for future realizations of these protocols and, accordingly, will benefit a variety of tasks in high-dimensional quantum information processing [25–28].

This work was supported by the Brazilian agencies CNPq (Grant No. 485401/2013-4), FAPEMIG (Grant No. APQ-00149-13), and PRPq/UFMG (Grant No. ADRC-01/2013). M. A. S-P., O. J., and A. D. acknowledge financial support from Millennium Scientific Initiative (Grant No. RC130001) and FONDECyT (Grants No. 1140635 and No. 11121318).

---

[*] msolisp@udec.cl
[†] lneves@fisica.ufmg.br

[1] R. W. Spekkens, Phys. Rev. A **75**, 032110 (2007).
[2] M. S. Leifer, Phys. Rev. Lett. **112**, 160404 (2014).
[3] C. Branciard, Phys. Rev. Lett. **113**, 020409 (2014).
[4] M. Ringbauer, B. Duffus, C. Branciard, E. G. Cavalcanti, A. G. White, and A. Fedrizzi, Nat. Phys. **11**, 249 (2015).
[5] N. Gisin, G. Ribordy, W. Tittel, and H. Zbinden, Rev. Mod. Phys. **74**, 145 (2002).
[6] F. Grosshans, G. Van Assche, J. Wenger, R. Brouri, N. J. Cerf, and P. Grangier, Nature (London) **421**, 238 (2003).
[7] For reviews of quantum-state discrimination see A. Chefles, Contemp. Phys. **41**, 401 (2000); S. M. Barnett and S. Croke, Adv. Opt. Photonics **1**, 238 (2009); J. A. Bergou, J. Mod. Opt. **57**, 160 (2010).
[8] A. S. Holevo, J. Multivariate Anal. **3**, 337 (1973).
[9] H. P. Yuen, R. S. Kennedy, and M. Lax, IEEE Trans. Inf. Theory **21**, 125 (1975).
[10] C. W. Helstrom, *Quantum Detection and Estimation Theory* (Academic, New York, 1976).
[11] I. D. Ivanovic, Phys. Lett. **123A**, 257 (1987).
[12] A. Chefles and S. M. Barnett, Phys. Lett. A **250**, 223 (1998).
[13] S. Croke, E. Andersson, S. M. Barnett, C. R. Gilson, and J. Jeffers, Phys. Rev. Lett. **96**, 070401 (2006).
[14] O. Jiménez, M. A. Solís-Prosser, A. Delgado, and L. Neves, Phys. Rev. A **84**, 062315 (2011).
[15] H. Sugimoto, Y. Taninaka, and A. Hayashi, Phys. Rev. A **86**, 042311 (2012).
[16] U. Herzog, Phys. Rev. A **86**, 032314 (2012).
[17] E. Bagan, R. Muñoz-Tapia, G. A. Olivares-Rentería, and J. A. Bergou, Phys. Rev. A **86**, 040303(R) (2012).
[18] K. Nakahira, T. S. Usuda, and K. Kato, Phys. Rev. A **86**, 032316 (2012).
[19] S.-H. Tan, B. I. Erkmen, V. Giovannetti, S. Guha, S. Lloyd, L. Maccone, S. Pirandola, and J. H. Shapiro, Phys. Rev. Lett. **101**, 253601 (2008).
[20] S. Pirandola, Phys. Rev. Lett. **106**, 090504 (2011).
[21] R. Nair and B. J. Yen, Phys. Rev. Lett. **107**, 193602 (2011).
[22] S. Lloyd, V. Giovannetti, and L. Maccone, Phys. Rev. Lett. **106**, 250501 (2011).
[23] P. van Loock, T. D. Ladd, K. Sanaka, F. Yamaguchi, K. Nemoto, W. J. Munro, and Y. Yamamoto, Phys. Rev. Lett. **96**, 240501 (2006).
[24] M. Ban, K. Kurokawa, R. Momose, and O. Hirota, Int. J. Theor. Phys. **36**, 1269 (1997).
[25] S. J. D. Phoenix, S. M. Barnett, and A. Chefles, J. Mod. Opt. **47**, 507 (2000).
[26] L. Roa, A. Delgado, and I. Fuentes-Guridi, Phys. Rev. A **68**, 022310 (2003); L. Neves, M. A. Solís-Prosser, A. Delgado, and O. Jiménez, Phys. Rev. A **85**, 062322 (2012).
[27] M. A. Solís-Prosser, A. Delgado, O. Jiménez, and L. Neves, Phys. Rev. A **89**, 012337 (2014).
[28] A. K. Pati, P. Parashar, and P. Agrawal, Phys. Rev. A **72**, 012329 (2005).
[29] R. L. Cook, P. J. Martin, and J. M. Geremia, Nature (London) **446**, 774 (2007).
[30] S. M. Barnett and E. Riis, J. Mod. Opt. **44**, 1061 (1997).
[31] R. B. M. Clarke, V. M. Kendon, A. Chefles, S. M. Barnett, E. Riis, and M. Sasaki, Phys. Rev. A **64**, 012303 (2001).
[32] G. Waldherr, A. C. Dada, P. Neumann, F. Jelezko, E. Andersson, and J. Wrachtrup, Phys. Rev. Lett. **109**, 180501 (2012).
[33] M. Fujiwara, M. Takeoka, J. Mizuno, and M. Sasaki, Phys. Rev. Lett. **90**, 167906 (2003).
[34] N. J. Cerf, M. Bourennane, A. Karlsson, and N. Gisin, Phys. Rev. Lett. **88**, 127902 (2002).
[35] L. Sheridan and V. Scarani, Phys. Rev. A **82**, 030301(R) (2010).
[36] M. Huber and M. Pawłowski, Phys. Rev. A **88**, 032309 (2013).
[37] S. Kochen and E. P. Specker, J. Math. Mech. **17**, 59 (1967).
[38] T. Vértesi, S. Pironio, and N. Brunner, Phys. Rev. Lett. **104**, 060401 (2010).
[39] L. Neves, G. Lima, J. G. Aguirre Gómez, C. H. Monken, C. Saavedra, and S. Pádua, Phys. Rev. Lett. **94**, 100501 (2005).
[40] P.-X. Chen, J. A. Bergou, S.-Y. Zhu, and G.-C. Guo, Phys. Rev. A **76**, 060303(R) (2007).
[41] See Supplemental Material at http://link.aps.org/supplemental/10.1103/PhysRevLett.118.100501, which includes Refs. [42–47], for more information about the experimental setup and data analysis.

[42] A. Márquez, I. Moreno, C. Iemmi, J. Campos, and M. J. Yzuel, Opt. Eng. **46**, 114001 (2007).

[43] I. Moreno, C. Iemmi, A. Márquez, J. Campos, and M. J. Yzuel, Appl. Opt. **43**, 6278 (2004).

[44] A. Lizana, A. Márquez, L. Lobato, Y. Rodange, I. Moreno, C. Iemmi, and J. Campos, Opt. Express **18**, 10581 (2010).

[45] I. D. Ivanovic, J. Phys. A **14**, 3241 (1981).

[46] D. F. V. James, P. G. Kwiat, W. J. Munro, and A. G. White, Phys. Rev. A **64**, 052312 (2001).

[47] G. Lima, L. Neves, R. Guzmán, E. S. Gómez, W. A. T. Nogueira, A. Delgado, A. Vargas, and C. Saavedra, Opt. Express **19**, 3542 (2011).

[48] M. Mohseni, A. M. Steinberg, and J. A. Bergou, Phys. Rev. Lett. **93**, 200403 (2004).

[49] P. J. Mosley, S. Croke, I. A. Walmsley, and S. M. Barnett, Phys. Rev. Lett. **97**, 193601 (2006).

[50] M. A. Solís-Prosser, A. Arias, J. J. M. Varga, L. Rebón, S. Ledesma, C. Iemmi, and L. Neves, Opt. Lett. **38**, 4762 (2013).

[51] J. J. M. Varga, L. Rebón, M. A. Solís-Prosser, L. Neves, S. Ledesma, and C. Iemmi, J. Phys. B **47**, 225504 (2014).

[52] M. A. Solís-Prosser and L. Neves, Phys. Rev. A **84**, 012330 (2011).

[53] A. Chefles, Phys. Rev. A **66**, 042325 (2002).

[54] The way we have parametrized the state coefficients for $D = 2$ to 9 and given that they were randomly selected for $D = 10$ to 21 ensure that our experiment did not restrict itself to a particular subset of symmetric states, encompassing, instead, sets constructed from arbitrary fiducial states [$|\psi_0\rangle$ in Eq. (1)].

[55] R. Fickler, M. Krenn, R. Lapkiewicz, S. Ramelow, and A. Zeilinger, Sci. Rep. **3**, 1914 (2013).

[56] L. Zhang, L. Neves, J. S. Lundeen, and I. A. Walmsley, J. Phys. B **42**, 114011 (2009).

[57] C. Scarcella, A. Tosi, F. Villa, S. Tisa, and F. Zappa, Rev. Sci. Instrum. **84**, 123112 (2013).

[58] M. Unternährer, B. Bessire, L. Gasparini, D. Stoppa, and A. Stefanov, Opt. Express **24**, 28829 (2016).